Journal of Ultrafine Grained and Nanostructured Materials
https://jufgnsm.ut.ac.ir
Vol. 55, No.2, December 2022, pp. 112-121
Print ISSN: 2423-6845 Online ISSN: 2423-6837
DOI: 10.22059/jufgnsm.2022.02.03

The effect of ball-milling parameters on the structures of Ti_3AlC_2 MAX phase and resultant $Ti_3C_2T_x$ MXene

Zahra Ahmadian[1], Mohammad Javad Azad[1], Somayeh Mohammadi*[,2], Yadollah Mortazavi[1], Abbas Ali Khodadadi[1]

[1]Catalysis and Nanostructured Materials Research Laboratory, School of Chemical Engineering, College of Engineering, University of Tehran, Tehran, Iran;
[2]School of Engineering science, College of Engineering, University of Tehran, Tehran, Iran.

Recieved: 29 September 2022; Accepted: 26 November 2022

**Corresponding author email: so.mohammadi@ut.ac.ir*

ABSTRACT

In this work, the effects of ball-milling parameters on the structure of the Ti_3AlC_2 MAX-phase, the precursor of $Ti_3C_2T_x$ MXene, is investigated. To clarify this effect, three approaches with different milling parameters were used to synthesize Ti_3AlC_2 MAX-phase. In all approaches, the initial elements with the proportion of 3Ti:1.3Al:1.9C were milled at different milling times, intervals, and rotating speeds. The resulting powders were sintered in a SPS furnace with the sintering temperature of 1000-1150 °C. According to our observation, emerging intermediate Ti and Al compounds in the milling process is the key point for forming the final Ti_3AlC_2 since such compounds would assist the formation of MAX-phase in the SPS process. Moreover, the temperature increment during the milling process is necessary for the formation of such intermediate compounds. This condition can be achieved when the ratio of intervals to milling times in each milling step is low enough (5 min per 30 min) or the rotating speed is high enough (around 600 rpm). The Al layers in Ti_3AlC_2 MAX-phase obtained in each approach are etched by HF solution to reveal the difference between the resultant $Ti_3C_2T_x$ MXene nanolayers. Our characterization suggests that ball-milling at 400 rpm for 18 hours with 5-minute intervals produces the highest quality MAX-phase and MXene.

Keywords: *ball-milling, Ti_3AlC_2 MAX-phase, $Ti_3C_2T_x$ MXene nanolayers, SPS method*

1. Introduction

Transition metal carbides, carbonitrides, and nitrides (MXenes) are among the most recent additions to the universe of two-dimensional materials. 2D materials have been found to have a wide variety of fascinating physical and chemical properties such as large specific surface area, excellent electrical and thermal conductivity, hydrophilic behavior, environmental stability, and favorable flexibility [1, 2]. According to their excellent performances, MXenes became one of the most famous candidates for many applications, including electrochemical energy storage in Li-ion, Li-S, Na-ion batteries, supercapacitors, medicine, electromagnetic interference shielding, gas sensing, water purification, electro/photo catalysts [3].

These family of materials have the layered structure and general formula of $M_{n+1}X_nT_x$, where M is an early transition metal (Sc, Ti, V, Cr, Zr), X is carbon and/or nitrogen, n = 1, 2, or 3, and T_x presents the surface termination groups such as –F, –OH, or –O [4]. Commonly, MXenes are produced from the selective etching of $M_{n+1}AX_n$ phase materials by fluoride-containing acidic solutions,

where A can be Al, Si, P, S, Ga [5].

$Ti_3C_2T_x$ is the first introduced and most studied MXene produced by selective etching of Al from Ti_3AlC_2 by HF acid at Drexel university in 2011 for the first time [5]. In 2014, $Ti_3C_2T_x$ MXene was produced using a HF-containing etchant such as ammonium bifluoride (NH_4HF_2) salt [6]; and later in the same year, $Ti_3C_2T_x$ "clay" was synthesized by taking advantage of making in situ HF by adding lithium fluoride (LiF) salt to hydrochloric acid (HCl) [7]. In 2016, larger single $Ti_3C_2T_x$ flakes were isolated by using the minimally intensive layer delamination (MILD) method [8].

The synthesis of Ti_3AlC_2 as a precursor of $Ti_3C_2T_x$, was first reported in 1994 by Pietzka and Schuster through sintering cold-compacted powder mixtures of titanium, TiAl, Al_4C_3 and carbon [9]. A variety of sintering methods, such as hot isostatic pressing (HIP) [10], hot-pressing (HP) [11], high-temperature annealing, self-propagating high-temperature synthesis (SHS) [12, 13], and spark plasma sintering (SPS) have been used to synthesize Ti_3AlC_2 [14-17]. In the above sintering methods, excluding SPS, the sintering temperature is high (1200 -1700 C), and/or the holding time is long (several hours). For instance, in the pressure less high-temperature annealing from elemental powders (Ti/Al/C) method, the annealing temperature and holding time are 1650 ˚C and 7.5 h, respectively[18].

Spark plasma sintering (SPS) is a rapid process for ceramic sintering with a lower temperature and less holding time. This method is similar to the hot-pressing process to some extent. Though, there is a crucial difference in the heat production mechanism at the microscopic level. In the SPS method, the powder is put in a graphite die and an instantaneous pulsed direct current is applied through the electrodes existing at the top and bottom of the graphite die. Such a current leads to a spark discharge through microscopic voids existing between the particles. Thereby, the surface of the particles is ignited and purified, and a self-heating phenomenon occurs between the particles[19-21].

Considering the issues mentioned for the other methods, the combination of mechanical ball milling and thermal heat treatment has attracted much interest. In this method, Mechanical ball-milling is preferred to be done before the SPS process to reach a superfine structure and increase the activity of the particles. It should be noted that both the ball-milling [22, 23], and the SPS parameters play a significant role in the quality of the final Ti_3AlC_2 MAX-phase [19-24].

Mechanical alloying is fundamentally a dry and high-energy ball milling process used to synthesize various alloys and intermetallic compounds. According to previous research which has used a combination of high energy ball milling and high-temperature heat treatment, the most frequently used condition for the ball mill procedure was 10-20 h and 400-500 rpm. For example, Yang et al. [25] synthesized Ti_3AlC_2 by spark plasma sintering of mechanically alloyed products from elemental powders of Ti, Al and C. In their work, the milling time, rotational speed, and the weight ratio of balls to powder were 9.5 h, 400 rpm and 10:1, respectively. Yang et al. [26] also fabricated Ti_3AlC_2 powder by a combination of high energy milling and heat treatment with Ti, C and Al as starting materials [26]. They found that after 24 h ball milling at 500rpm new phases, including Ti_3AlC_2, Ti-Al intermetallic and TiC, were formed. In the next step to achieve high purity Ti_3AlC_2, a heat treatment process with different temperature from 500-1100˚C was applied. Their results indicated that when the temperature increased to 1100 ˚C, the final reactions between Ti-Al intermetallic and TiC resulted in high purity Ti_3AlC_2 [26]. Recently, Gao et. al [27] synthesized Ti_3AlC_2 using Ti/Al/C powders as the starting materials by ball-milling (10h at the rotating speed of 200 rpm) and under different conditions of SPS. Their experimental results showed that the most efficient condition for fabricating high purity Ti_3AlC_2 was 3:1.2:1 for the proportion of raw powders and 1300˚C for the SPS temperature.

In this work, the influence of ball-milling parameters on the quality of the final Ti_3AlC_2 MAX-phase and resultant $Ti_3C_2T_x$ MXene nanolayers was investigated. Three approaches with different ball-milling conditions were employed to synthesize Ti_3AlC_2 MAX-phase. We used these approaches to provide three levels of energy in the milling process: low energy, high-energy and harsh. In all cases, the milling times between intervals were 30 minutes. In the first (low energy) approach, the intervals between the milling times were 20 minutes with a rotating speed of 400 rpm leading to the process temperature being near room temperature. In the second (high energy) approach, the intervals were decreased to 5 minutes, which resulted in temperature increment. Finally, in the third approach, which was called

harsh ball-milling, the rotational speed of the cup increased up to 600 rpm while the total milling time was decreased to 4 h. In this approach, the total energy received by the powders is much higher than in the two previous approaches. The ball-milled powders are then sintered through the SPS process. The ball-milled and SPS products are characterized using SEM, EDS, and XRD analysis to understand the effect of ball-milling parameters on the formation of Ti_3AlC_2 MAX-phase and resultant MXene nanosheets. According to our observation, emerging of intermediate Ti and Al compounds in the milling process is a key point for the formation of final Ti_3AlC_2 since the presence of such compounds would assist the formation of MAX-phase in the SPS process. It is also realized that the temperature increment during the milling process is necessary for the formation of such intermediate compounds. The Al layers of the obtained MAX phase powders were etched by HF solution to achieve $Ti_3C_2T_x$ MXene nano-layers. It was observed that by increasing the rotational speed in the milling process, the final resultant MXene nano-sheets become smaller in size. By comparing the MXene nano-sheets obtained through high energy and harsh approaches, it can be implied that the milling parameters would be optimal if the intervals between the milling steps are minimum and the rotational speed is 400 rpm. According to our results, the highest quality of synthesized MAX-phase and MXene is observed when the ball-milling process is performed at a medium speed (400 rpm) with the lowest interval (5 minutes per 30 seconds).

2. Experimental details

2.1. Materials

Titanium (99.7%pure, 45μm), Al (99.5%pure, 25 μm) and graphite (99.8%pure,5–6 μm)) powders were purchased. Hydrofluoric acid (HF, 38-40 wt%) was also purchased from Merck company. All of the reagents and supplies were utilized just as they were obtained, with no further purification.

2.2. Synthesis of Ti_3AlC_2 Max phase

The proportion of raw materials was the same in all three approaches (3Ti:1.3Al:1.9C). According to the chemical formula of Ti_3AlC_2, the atomic ratio of the raw materials is expected to be 3Ti:1Al:2C. However, during the milling process, there is a loss of Al due to its high vapor pressure and low melting point. According to our observation and referring to the other reported works [1-2,4-5], we examined the different ratios of raw materials and found out that the ratio of 3Ti:1.3Al:1.9C would result in a high-quality MAX phase. The powder mixtures were put in the steel jars under Argon protective atmosphere, and the weight ratio of balls to powders was 10:1. The Mechanical milling process was conducted by high-energy ball milling at a different time and rotational speed.

Three approaches with different ball-milling conditions were employed to synthesize Ti_3AlC_2 MAX-phase. We used these approaches to provide three levels of energy in the milling process: low energy, high energy and harsh.

In the first approach, the raw powders were milled at 400 rpm with a total time of 10 and 18 h with the same sequential steps of 30 minutes milling and 20 minutes interval (low energy). In the second approach, the raw powders were milled at 400 rpm for 18 h with an interval of 5 minutes (high energy). In the third approach, raw powders were milled at 600 rpm for 4 h continuously with no interval, which can be considered a harsh ball-milling process.

Based on previous works [4, 19, 25], For all cases, the mechanically milled elemental powders were placed in cylindrical graphite die with an inner diameter of 25 mm to sinter in a spark plasma-sintering furnace. The heating rate of the furnace was set to 80 °C/min, and the sintering temperature was set at 1000-1150 °C. In this process, the soaking time was 10 minutes, and the constant axial pressure was 35MPa.

2.3. Synthesis of $Ti_3C_2T_x$ MXene nanosheets

According to the procedure reported before, Selective etching of Al from Ti_3AlC_2 MAX-phase with HF solution was done to yield $Ti_3C_2T_x$ MXene nanosheets [5]. 0.5 gr of Ti_3AlC_2 was slowly added into a PET bottle containing 10 mL of 10 wt% HF solution, which was magnetically stirred continuously for 36 h at room temperature. The speed of the Stirrer was set to 400 rpm. In each method, the reacted solutions were washed with deionized water and centrifuged at 3500 rpm for 5 min, several times, until the pH of the black result supernatant reached 5-6. The final powder was dried for 12 h at 60°C in a vacuum oven.

2.4. Material characterization

X-ray diffraction (XRD) patterns were obtained with a powder diffractometer (Rigaku Ultima,

Japan) using Cu K α radiation with a step scan of 0.02 ° and a rate of 4˚/minutes. In order to obtain high-magnification images of the treated powders and observe the morphology of the samples, scanning electron microscope, (FESEM, HITACHI S4160, JAPAN) was used.

3. RESULT AND DISCUSSION

3.1. First approach: ball-milling with the rest intervals of 20 minutes

Fig. 1-(a) shows the X-ray diffraction patterns of the ball-milled samples at different milling times of 10 h (the red diagram) and 18 h (the blue diagram) with the milling steps of 30 minutes and rest intervals of 20 minutes at 400 rpm. In these diagrams, the peaks of Ti at 2θ = 35.2˚, 38.39˚, 40˚, 53˚, 63.1˚, 70.8˚, 76.3˚ and Al at 2θ = 38.39˚, 44.65˚, 65.5˚, 78.4˚ could be observed [23-26]. However, no distinctive peak of Carbon is visible in the XRD patterns implying that graphite has been transformed to amorphous Carbon or distributed in the grain boundaries of Ti [23]. In the XRD pattern of both samples, only the peaks of elemental powders can be detected, which indicates that no specific reaction between the reactants has occurred. It seems that the long intervals (20 min) between the milling steps did not allow the average temperature during the whole milling process to rise enough to reach the required temperature for the possible reactions [26]. Therefore, we could only distinguish the initial powders (Ti, Al, and C) in the XRD patterns, and no intermediate compounds were found. It is worth mentioning that by increasing the milling time to even 24 h, still, no reactions took place between the elemental powders. SEM micrographs of the two ball-milled samples with milling times of 10 and 18 h (Fig. 1-(b, c)) show that during the milling process, the average size of C and Al particles are deceased, but Ti sheets are still present with the large size (above 20μm). However, the size of the Ti flakes has decreased in the latter.

Both ball-milled powders were sintered by the SPS process at 1100 ˚C. The XRD pattern and SEM images of the sintered samples are depicted in Fig. 2. In the XRD pattern presented in Fig. 2-(a), distinctive peaks of TiC at 2θ = 35.9˚, 42˚, 60.9˚, 72.9˚ and 76.9˚ are observed [23,26]. Although several diffraction peaks of Ti_3AlC_2 are also visible in this pattern, some of them are in common with TiC peaks and the main peak of Ti_3AlC_2 which is located in 2θ=9.6˚ and refers to the layered structure of Ti_3AlC_2 is not recognized. In addition, the peaks of Al_2O_3 at 2θ=43.37˚, 53.31˚ and Ti_2AlC at 2θ=13.2˚, 34.3˚, 39.6˚, 53.35˚ are detectable [26]. Moreover, due to the interaction between Ti

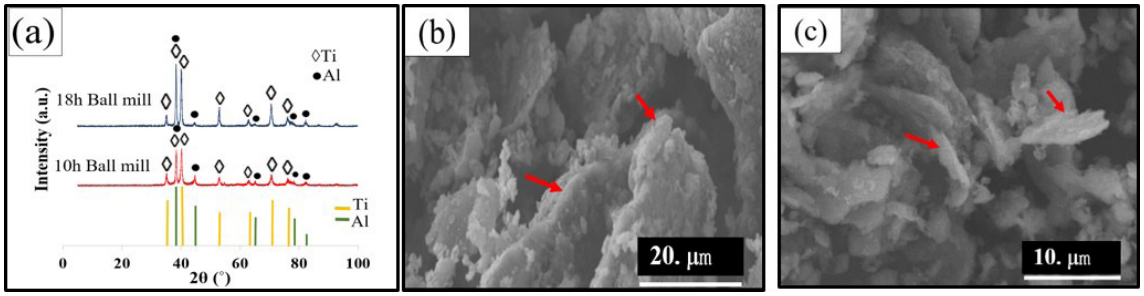

Fig. 1- (a) XRD patterns of the 3Ti/1.3Al/1.9C powder mixture after 10h and 18h ball-milling with the milling steps of 30 minutes and rest intervals of 20 minutes at 400 rpm. The SEM micrograph of the ball-milled samples for (b) 10 h and (c) 18 h.

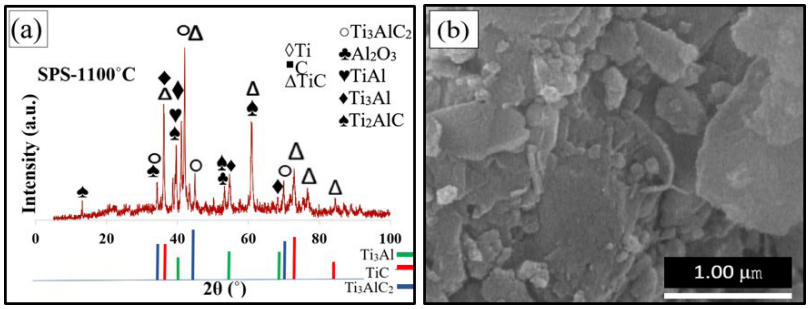

Fig. 2- (a) XRD pattern and (b) SEM micrograph of as-sintered powder by the SPS method at 1100˚C in the first approach.

and Al, Ti-Al intermetallic phases like Ti_3Al and TiAl are formed which the peaks at 2θ =36.19˚, 39.39˚, 39.53˚, 41.07˚, 54.63˚, 68.15˚ correspond to these compounds [28, 29]. In the SEM image in Fig. 2-(b), no MAX-phase zone is visible which corresponds with the XRD result.

The possible reactions in the SPS process are illustrated in eq. 1-5[19]. According to the XRD result presented in Fig. 2-(a), it seems that during the SPS process, the intermediate compounds like TiC and Ti_3Al are formed through the reactions presented by eq. 1-2. However, the reactions presented by eq. 3-5 do not take place to result the formation of Ti_3AlC_2.

$$Ti + C \rightarrow TiC \quad (1)$$
$$4Ti + 2Al \rightarrow Ti_3Al + TiAl \quad (2)$$
$$Ti_3Al + C \rightarrow Ti_3AlC \quad (3)$$
$$Ti_3AlC + 2TiAl + TiC + C \rightarrow 3Ti_2AlC \quad (4)$$
$$Ti_2AlC + TiC \rightarrow Ti_3AlC_2 \quad (5)$$

It is worth mentioning that even by increasing the sintering temperature to 1150˚C and 1200˚, the Ti_3AlC_2-MAX phase was not formed. It can be concluded that due to the lack of intermediate compounds in the milling products, as determined by the XRD result in Fig. 1-(a), the of these compounds during the SPS process, would not be effective in the formation of Ti_3AlC_2 in the same process.

3.2. Second approach: ball-milling with the rest intervals of 5 minutes

The red diagram in Fig. 3-(a) presents the XRD pattern of the ball-milled sample with the milling steps of 30 minutes and rest intervals of 5 minutes.

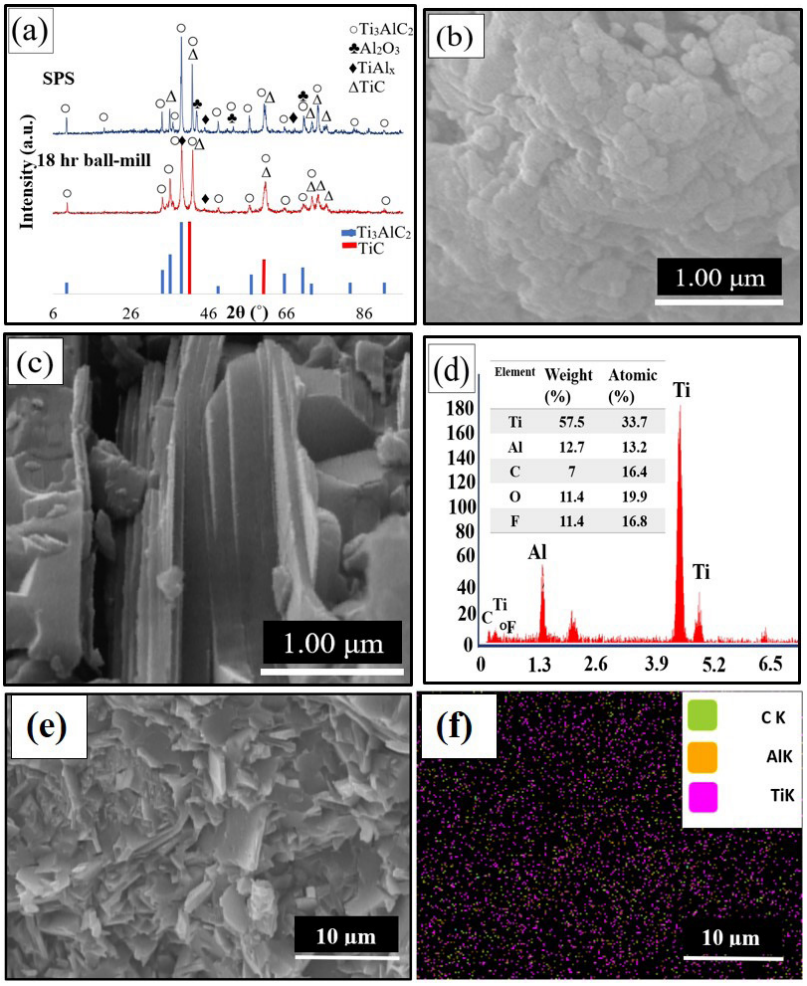

Fig. 3- (a) XRD patterns of the 3Ti/1.3Al/1.9C powder mixture after 18h ball-milling at 400 rpm with the intervals of 5 minutes (red diagram) and after SPS at 1100˚C (blue diagram), SEM micrograph of the sample (b) after ball-milling, (c), (d) EDX result of the sample after SPS, (e) SEM image and (f) its corresponding EDS mapping of the of the sample after SPS.

The rotational speed of the milling process was 400 rpm and the overall milling time was 18 h. According to the XRD diagram, a noticeable amount of Ti_3AlC_2 has already been formed by mechanical milling since the main peaks of Ti_3AlC_2 at 2θ = 9.5˚, 39˚, 42˚, and 60.44˚ are detectable [19, 22, 24]. Furthermore, the distinctive peaks of TiC at 2θ = 35.9˚, 42˚ and 60.5˚ are present in the diagram [7, 23]. In addition, in contrast with approach 1, Ti-Al intermetallic phases were formed in the ball-milling process because the peaks related to these compounds can be seen at 2θ = 38.96˚ and 44.92˚[23]. It can be speculated that when the milling process is performed with low intervals between the milling steps, the average temperature of the powder is increased [19]. Consequently, the required energy for the formation of Ti_3AlC_2 is supplied. The SEM image of ball-milled powder by the second approach is presented in Fig. 3-(b). As shown in this image, the morphology of the milled powder is far different from that in approach 1. No Ti flakes are visible in this image, and the powder has a homogeneous morphology with an average grain size of 500 nm.

Like approach 1, the ball-milled powder was sintered by the SPS process at 1100 ˚C. The blue diagram in Fig. 3-(a) demonstrates the XRD pattern of this sample, which corresponds well to previously reported Ti_3AlC_2 XRD patterns [19, 30]. By comparing the XRD patterns in Fig. 3-(a), it is determined that the peak intensity ratio of Ti_3AlC_2 (at 2θ = 9.6˚) to TiC (at 2θ = 35.9˚) has increased from 0.3 in the milled powder to 1.1 in the sintered powder by SPS process. The SEM image of the sintered sample is depicted in Fig. 3-(c), in which Ti_3AlC_2 zones with a dense structure are clearly visible. According to EDS analysis as presented in Fig. 3-(d), the atomic percentage of Ti and Al is 33.7%, 13.2%, respectively. The atomic ratio of Ti to Al is 2.55 which is near the ratio of these elements in the chemical formula of Ti_3AlC_2. The EDS map of the sample with the corresponding SEM image depicted in Fig. 3-(e), is presented in Fig. 3-(f) which shows the distribution of elements in the sample.

3.3. Third approach: harsh ball-milling

In the third approach, a harsh ball-milling process was performed with a rotational speed of 600 rpm for 4 h with sequential milling times of 30 minutes and rest intervals of 5 minutes. The XRD pattern of the sample mechanically milled by harsh condition is presented in the red diagram in Fig. 4-(a). As mentioned in the previous approach, the appeared peaks at 2θ = 35.9˚, 42˚, 44.5˚, 60.5˚, 73˚, and 77˚ are the characteristic peaks of TiC, which indicates the formation of considerable amounts of TiC in the milled sample. It is noteworthy that Al and Ti peaks are still present at 2θ =42.37˚ and 44.8˚, respectively. According to Fig. 4-(a), diffraction peaks are broader in harsh-milled sample, which can imply that the size of the particles is smaller in the third approach. It seems that despite the lower milling time (4 h), due to the higher rotational speed (600 rpm), the required temperature and energy are provided to form the intermediate phases, which are mainly because of the intense colliding and friction between the balls and the jar wall [19].

The milled powder was sintered using the identical SPS condition of the previous approaches (1100 ˚C and 35 MPa). The blue diagram in Fig. 4-(a) illustrates the XRD pattern of the as-sintered sample. Similar to the second approach, the main peak of Ti_3AlC_2 at 2θ = 9.6 appeared in the XRD pattern indicating the formation of Ti_3AlC_2 MAX-phase [17,19].

The SEM image of the as-sintered sample is

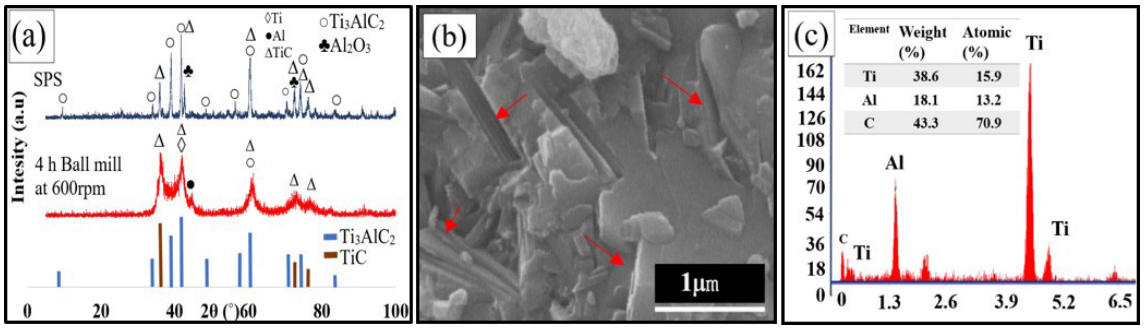

Fig. 4- (a) XRD patterns of the 3Ti/1.3Al/1.9C powder mixture after 4h ball-milling at 600 rpm with the rest intervals of 5 minutes (red diagram) and after SPS at 1100˚C (blue diagram), (b) SEM micrograph, and (c) EDX result of the powder after SPS at 1100 ˚C.

depicted in Fig. 4-(b) in which some of the Ti_3AlC_2 crystalline zones are pointed by the red arrows. By comparing the SEM image in this figure with the SEM image in Fig. 3-(c), it is observed that the structures of MAX-phases obtained in the second and third approaches are quite different. The MAX-phase structure of the third approach has more crushed parts and more sharp edges. The EDS result of the MAX-phase powder obtained in the third approach is depicted in Fig. 4-(c), which indicates the presence of initial elements in the powder. However, the ratio of Ti to Al does not correspond with the ratio of these elements in the chemical formula of Ti_3AlC_2, which can imply the presence of impurities in the powder.

The result of the third approach suggests that even by applying harsh condition in the ball-mill process, Ti_3AlC_2 can be formed. To be specific, only if the intermediate phases are synthesized during the milling process the SPS procedure would be effective for MAX-Phase fabrication.

3.4. Fabrication of MXene nanolayers

The prepared Ti_3AlC_2 powders are etched with HF solution to obtain $Ti_3C_2T_X$ MXene flakes. To investigate the difference between the resultant MXene in the second and third approaches, the MXene nanolayers are characterized by means of XRD and SEM.

The XRD pattern of $Ti_3C_2T_x$ powders derived from Ti_3AlC_2 in the second approach is shown in Fig. 5-(a). The peaks observed at 2θ=9.16˚, 18.6˚, 28˚, 35.96˚, 41.8˚, 60.56˚, 72.56˚, and 91.36˚ degrees are the characteristic peaks of $Ti_3C_2T_x$ [5]. On the other hand, the main peaks of Ti_3AlC_2 disappeared except that at 2θ=9.6˚, which is shifted towards lower angles. This shift can be attributed to the transformation of Ti_3AlC_2 to $Ti_3C_2T_x$ [22].

The SEM image of this sample is presented in Fig. 5-(b), where the layered structure of $Ti_3C_2T_x$ MXene is clearly visible. The typical flake size is 3-10 µm in this sample. For further investigation, the SEM image of $Ti_3C_2T_x$ sonicated for 30 minutes is presented in Fig. 5-(c). As stated in literature, various parameters like sonication, intercalants and concentration of HF etchant affect the exfoliation process [31]. In agreement with those reports, as is shown in Fig. 5-(c), the sonication process reduced the size of flacks to 0.3-0.5µm [31]. Moreover, the EDX result of $Ti_3C_2T_x$ powder in the second approach is shown in Fig. 5-(d) in which the percentage of Ti, Al, C, O, and F is 20.1%, 3.2%, 30.2%, 17.5%, and 29%, respectively, confirming selective removal of Al atoms from the structure and the presence of functional groups (-OH, -F, and -O) on the MXene structure. The distribution of the mentioned elements can be observed in the EDS mapping picture presented in Fig 5-(e).

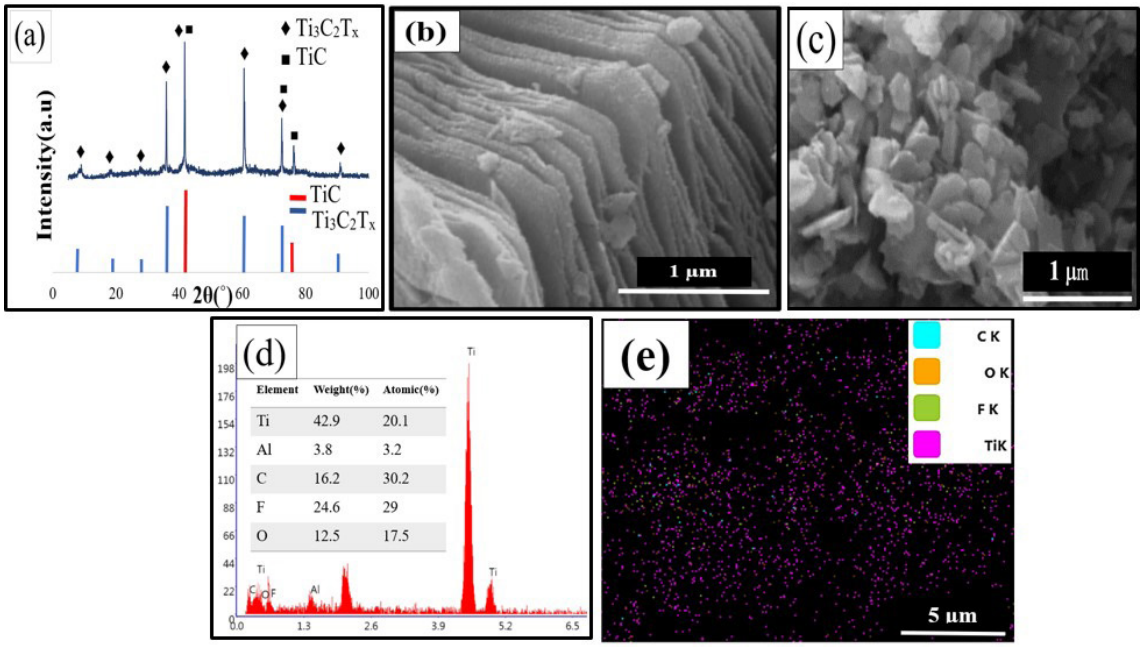

Fig. 5- (a) XRD patterns, and (b) SEM image of $Ti_3C_2T_x$ powder in the second approach. (c) SEM image of the $Ti_3C_2T_x$ Sonicated for 30 minutes. (d) EDS result and (e) EDS mapping of $Ti_3C_2T_x$ powder in the second approach.

Fig. 6-(a) shows the XRD pattern of $Ti_3C_2T_x$ powders derived from Ti_3AlC_2 in the third approach. Like the MXene produced in the second approach, the peaks observed at 2θ=17.38˚, 26.18˚, 36.14˚, 42.1˚, 60.86˚, 72.9˚, and 91.58˚ degrees are the characteristic peaks of $Ti_3C_2T_x$ which reveals the formation of the $Ti_3C_2T_x$ MXene [28, 29]. In addition, TiC peaks as impurities at 2θ= 41.98˚, 72.9˚, and 76.66˚ appeared. The SEM image of the resultant $Ti_3C_2T_x$ is presented in Fig. 6-(b). As depicted in this image, the typical size of the MXene nanoflakes is 0.1 to 0.5 µm. The morphology of these MXene nanolayers is similar to previously shown ultrasonicated and delaminated MXene layers in the second approach (Fig. 5-(c)). The smaller size and delaminated form of these layers can be attributed to the smaller MAX-phase zones in Ti_3AlC_2 powder from which these MXene nanolayers are derived. In other words, with the same etching time, if the Ti_3AlC_2 precursor consists of smaller grains, Al layers would be etched more efficiently. As a result, the resultant MXene nanolayers would be more delaminated and smaller. Generally, Ti_3AlC_2 MAX-phase has a polycrystalline structure where, each crystalline grain or zone consists of Ti, Al and C layers with the formula of Ti_3AlC_2. Basically, the size of the derived MXene layers should be the same as the size of the Ti-C layers in the crystalline zones of the MAX-phase material. On the other hand, by increasing the etching time, the derived MXene layers are more de-stacked and delaminated. The larger the size of a crystalline zone, the longer it takes to completely remove Al atoms and delaminate the MXene layers. Thus, during the same etching time, the MXene layers which obtained in the second approach are expected to be smaller and more delaminated. According to EDS analysis as presented in Fig. 6-(c), the percentage of Ti, Al, C, F, and O is 10.5%, 4.6%, 53.2%, 8.1%, and 23.6%, respectively, which indicates the successful removal of Al layers from the MXene structure. The distribution of these elements is depicted in the EDS mapping picture in Fig. 6-(d).

4. Conclusion

In this study, mechanical milling with different parameters was performed before the SPS process to investigate the effect of milling conditions on the synthesis of Ti_3AlC_2 MAX-phase. The Al layers of the obtained MAX phase powders were etched by HF solution to achieve $Ti_3C_2T_x$ MXene nano-layers. It was observed that different milling conditions result in different qualities of the synthesized MAX-phases. According to our observation, emerging intermediate Ti and Al compounds in the

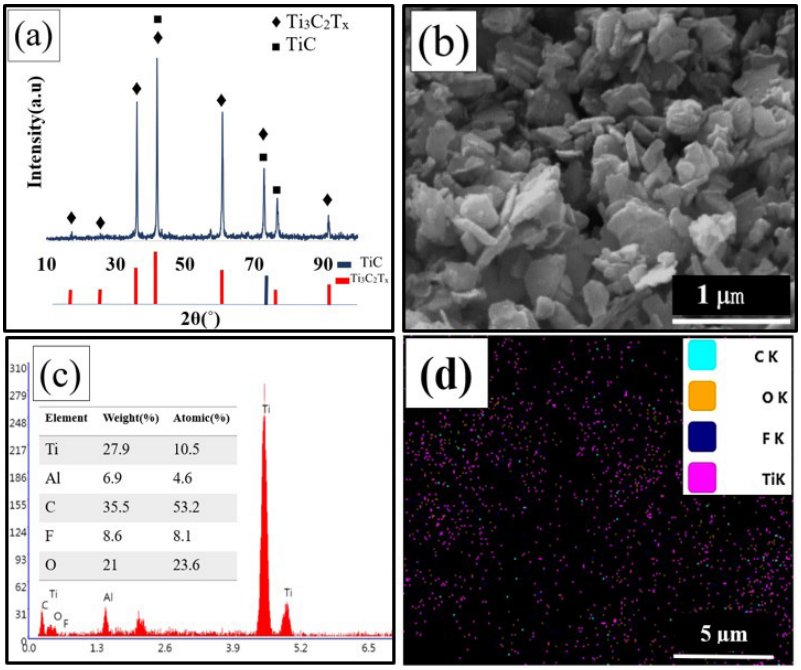

Fig. 6- (a) XRD patterns, and (b) SEM image of $Ti_3C_2T_x$ powder in the third approach. (c) EDS result and (d) EDS mapping picture of $Ti_3C_2T_x$ powder in the third approach.

milling process was a key point for the formation of final Ti_3AlC_2 since such compounds would assist the formation of the MAX-phase in the SPS process. It was also realized that the temperature increment during the milling process is necessary for the formation of intermediate compounds. By comparing the MXene nano-sheets obtained in different conditions, it can be implied that the milling parameters would be optimal if the intervals between the milling steps were minimum. According to our results, the highest quality of synthesized MAX-phase and MXene is observed when the ball-milling process is performed at a medium speed (400 rpm) with the lowest interval (5 minutes per 30 seconds).

Acknowledgment

The authors disclosed receipt of the following financial support for the research of this article: This work was supported by the Iran High-Tech Laboratory Network [grant number: LabsNet-24297].

References

1. Pan Z, Cao F, Hu X, Ji X. A facile method for synthesizing CuS decorated Ti3C2 MXene with enhanced performance for asymmetric supercapacitors. Journal of Materials Chemistry A. 2019;7(15):8984-92.
2. Ghosh NC, Harimkar SP. Consolidation and synthesis of MAX phases by Spark Plasma Sintering (SPS): a review. Advances in Science and Technology of Mn+1AXn Phases: Elsevier; 2012. p. 47-80.
3. Zhao L, Wang K, Wei W, Wang L, Han W. High-performance flexible sensing devices based on polyaniline/MXene nanocomposites. InfoMat. 2019;1(3):407-16.
4. Shuck CE, Han M, Maleski K, Hantanasirisakul K, Kim SJ, Choi J, Reil WE, Gogotsi Y. Effect of Ti3AlC2 MAX phase on structure and properties of resultant Ti3C2T x MXene. ACS Applied Nano Materials. 2019 May 13;2(6):3368-76.
5. Naguib M, Kurtoglu M, Presser V, Lu J, Niu J, Heon M, et al. Two-Dimensional Nanocrystals Produced by Exfoliation of Ti3AlC2. Advanced Materials. 2011;23(37):4248-53.
6. Halim J, Lukatskaya MR, Cook KM, Lu J, Smith CR, Näslund L-Å, et al. Transparent Conductive Two-Dimensional Titanium Carbide Epitaxial Thin Films. Chem Mater. 2014;26(7):2374-81.
7. Ghidiu M, Lukatskaya MR, Zhao M-Q, Gogotsi Y, Barsoum MW. Conductive two-dimensional titanium carbide 'clay' with high volumetric capacitance. Nature. 2014;516(7529):78-81.
8. Shahzad F, Alhabeb M, Hatter CB, Anasori B, Man Hong S, Koo CM, et al. Electromagnetic interference shielding with 2D transition metal carbides (MXenes). Science. 2016;353(6304):1137-40.
9. Pietzka MA, Schuster JC. Summary of constitutional data on the Aluminum-Carbon-Titanium system. Journal of Phase Equilibria. 1994;15(4):392-400.
10. Tzenov, N.V. and M.W. Barsoum, Synthesis and characterization of Ti3AlC2. Journal of the American Ceramic Society, 2000. **83**(4): p. 825-832.
11. Wang X, Zhou Y. Solid–liquid reaction synthesis of layered machinable Ti3AlC2 ceramic. Journal of Materials Chemistry. 2002;12(3):455-60.
12. Khoptiar Y, Gotman I, Gutmanas EY. Pressure-Assisted Combustion Synthesis of Dense Layered Ti3AlC2 and its Mechanical Properties. Journal of the American Ceramic Society. 2005;88(1):28-33.
13. Ge Z, Chen K, Guo J, Zhou H, Ferreira JMF. Combustion synthesis of ternary carbide Ti3AlC2 in Ti–Al–C system. Journal of the European Ceramic Society. 2003;23(3):567-74.
14. Yunus M, Kumar R, Maji BC, Krishnan M. An optimized method for synthesizing phase-pure Ti3AlC2 MAX-phase through spark plasma sintering. Journal of the European Ceramic Society. 2022;42(2):354-63.
15. Syrtanov M, Kashkarov E, Murashkina T, Travitzky N. Spark Plasma Sintering of Paper-Derived Ti3AlC2-Based Composites: Influence of Sintering Temperature. Materials Science Forum. 2021;1016:1790-6.
16. Zhou W, Mei B, Zhu J, Hong X. Synthesis of high-purity Ti3SiC2 and Ti3AlC2 by spark plasma sintering (SPS) technique. Journal of Materials Science. 2005;40(8):2099-100.
17. Zhou A, Wang C-A, Hunag Y. Journal of Materials Science. 2003;38(14):3111-5.
18. Apal'kova GD. Effect of Nano-Dispersed Iron Oxide Additions on Carbon Refractory Density Formation. Refractories and Industrial Ceramics. 2019;59(6):609-11.
19. Yang C, Jin S, Liang B, Liu G, Duan L, Jia S. Synthesis of Ti3AlC2 by spark plasma sintering of mechanically milled 3Ti/xAl/2C powder mixtures. Journal of Alloys and Compounds. 2009;472(1-2):79-83.
20. Gao L, Wang HZ, Hong JS, Miyamoto H, Miyamoto K, Nishikawa Y, et al. Mechanical Properties and Microstructure of Nano-SiC–Al2O3 Composites Densified by Spark Plasma Sintering. Journal of the European Ceramic Society. 1999;19(5):609-13.
21. Perera DS, Tokita M, Moricca S. Comparative study of fabrication of Si3N4/SiC composites by spark plasma sintering and hot isostatic pressing. Journal of the European Ceramic Society. 1998;18(4):401-4.
22. von Treifeldt JE, Firestein KL, Fernando JFS, Zhang C, Siriwardena DP, Lewis C-EM, et al. The effect of Ti3AlC2 MAX phase synthetic history on the structure and electrochemical properties of resultant Ti3C2 MXenes. Materials & Design. 2021;199:109403.
23. Li S-B, Zhai H-X, Bei G-P, Zhou Y, Zhang Z-L. Synthesis and microstructure of Ti3AlC2 by mechanically activated sintering of elemental powders. Ceramics International. 2007;33(2):169-73.
24. Zou Y, Sun Z, Hashimoto H, Tada S. Low temperature synthesis of single-phase Ti3AlC2 through reactive sintering Ti/Al/C powders. Materials Science and Engineering: A. 2008;473(1-2):90-5.
25. Yang C, Jin SZ, Liang BY, Jia SS. Low-temperature synthesis of high-purity Ti3AlC2 by MA-SPS technique. Journal of the European Ceramic Society. 2009;29(1):181-5.
26. Zhu JF, Qi GQ, Yang HB, Wang F. Synthesis of Ti3AlC2 Powder by High Energy Ball Milling and High Temperature Heat Treatment. InMaterials Science Forum 2010 (Vol. 658, pp. 181-184). Trans Tech Publications Ltd.
27. Zhu JF, Qi GQ, Yang HB, Wang F. Synthesis of Ti3AlC2 Powder by High Energy Ball Milling and High Temperature Heat Treatment. InMaterials Science Forum 2010 (Vol. 658, pp. 181-184). Trans Tech Publications Ltd.
28. Ronnasi B, Mahmoodian M, Mohammadi S, Yasoubi M, Sanaee Z.-NSA doped PPy @ Ti3C2Tx hybrid material as a high-performance supercapacitor electrode. Journal of Materials Research. 2022;37(22):3965-75.

29. Chen B, Feng A, Liu K, Wu J, Yu Y, Song L. Subsize Ti3C2T derived from molten-salt synthesized Ti3AlC2 for enhanced capacitive deionization. Ceramics International. 2021;47(3):3665-70.
30. Gao L, Han T, Guo Z, Zhang X, Pan D, Zhou S, et al. Preparation and performance of MAX phase Ti3AlC2 by in-situ reaction of Ti-Al-C system. Advanced Powder Technology. 2020;31(8):3533-9.
31. Munir S, Rasheed A, Rasheed T, Ayman I, Ajmal S, Rehman A, et al. Exploring the Influence of Critical Parameters for the Effective Synthesis of High-Quality 2D MXene. ACS Omega. 2020;5(41):26845-54.